

(1)



AD A11 3688

CHARACTERIZATION OF RAPIDLY SOLIDIFIED ALLOYS

D. SHECHTMAN AND E. HOROWITZ

APPROVED FOR PUBLIC RELEASE  
DISTRIBUTION IS UNLIMITED

THE JOHNS HOPKINS UNIVERSITY  
CENTER FOR MATERIALS RESEARCH  
BALTIMORE, MARYLAND 21218

DTIC FILE COPY

DISTRIBUTION STATEMENT A  
Approved for public release;  
Distribution Unlimited

JANUARY 1982

DTIC  
ELECTED  
APR 19 1982  
H

82 04 19 076

(1)

CHARACTERIZATION OF RAPIDLY SOLIDIFIED ALLOYS

D. SHECHTMAN AND E. HOROWITZ

THE JOHNS HOPKINS UNIVERSITY  
CENTER FOR MATERIALS RESEARCH  
BALTIMORE, MARYLAND 21218

DISTRIBUTION STATEMENT A

Approved for public release;  
Distribution Unlimited

JANUARY 1982

DTIC  
ELECT  
APR 19 1982  
H

AO 4344

ARPA ORDER NO.

~~MDA-903-81-C-0555~~

NAME OF CONTRACTOR:

The Johns Hopkins University  
Center for Materials Research  
Baltimore, Maryland 21218

EFFECTIVE DATE OF CONTRACT:

08-01-81

CONTRACT EXPIRATION DATE:

07-31-83

REPORTING PERIOD:

08-01-81 to 01-01-82

CONTRACT NO.

MDA 903-81-C-0555

PRINCIPAL INVESTIGATOR:

Dr. Emanuel Horowitz, 301-338-7916

SHORT TITLE OF WORK:

Characterization of Rapidly  
Solidified Alloys

SPONSORED BY

DEFENSE ADVANCED RESEARCH PROJECTS AGENCY (DoD)

ARPA ORDER NO. ~~MDA-903-81-C-0555~~

4344

UNDER CONTRACT NO. MDA-903-81-C-0555

DEPARTMENT OF THE ARMY, DEFENSE SUPPLY SERVICE

WASHINGTON, D. C. 20310

"The views and conclusions contained in this document are those of the authors and should not be interpreted as representing the official policies, either expressed or implied, of the Defense Advanced Research Projects Agency or the U. S. Government."

# TABLE OF CONTENTS

	<u>PAGE</u>
Abstract	v
I. Metastable Phases in the Aluminum-Iron System	1
A. Introduction	1
B. Al 18 <sup>W</sup> /o Fe	2
C. Al 25.7 <sup>W</sup> /o Fe	6
D. Al 34.1 <sup>W</sup> /o Fe	7
E. Discussion	8
II. The Crystallization of Pd <sub>77</sub> Si <sub>17</sub> Cu <sub>6</sub>	9
III. Rapidly Solidified Powders Generated by the Micro Particle Processor (Phrasor)	10
IV. References	13
V. Appendix 1 (Figures 1-26)	14



Accession For	
NTIS GRA&I	<input checked="" type="checkbox"/>
DTIC TAB	<input type="checkbox"/>
Unannounced	<input type="checkbox"/>
Justification	<i>per</i>
By	<i>see</i>
Distribution/	
Availability Codes	
Dist	Avail and/or Special
<i>A</i>	

## TABLES

	<u>PAGE</u>
Table 1. Spinning Conditions for Al 18 <sup>W</sup> /o Fe	2
Table 2. Heat Treatments of Ribbon #3	2
Table 3. The Ring Diameters Shown in Figure 16 and the Corresponding d Spacings	6

## APPENDIX 1

- Figure 1. The globular phase in Al 18 wt % Fe (ribbon #1)
- Figure 2. Selected area diffraction ring pattern from ribbon #1
- Figure 3.  $Al_3Fe$  particle in ribbon #3
- Figure 4. The globular phase in ribbon #3
- Figure 5. Microdiffraction from globular phase - crystalline
- Figure 6. Microdiffraction from globular phase - microcrystalline
- Figure 7. Microcrystallites formed in globular phase
- Figure 8. Composition of the globular phase (EDAX on STEM)
- Figure 9. Composition of matrix (cells and cell boundaries) (EDAX on STEM)
- Figure 10. Lattice imaging of ordered globules in ribbon #3 (300°C-10h)
- Figure 11. First  $Al_3Fe$  needles to appear in ribbon #3 (400°C-1h)
- Figure 12.  $Al_3Fe$  in Al matrix is characteristic of ribbon #3 after 8 hours at 400°C
- Figure 13. Ribbon #3, 1 hour at 500°C, Al matrix and  $Al_3Fe$  but some globules still exist
- Figure 14.  $Al_3Fe$  in Al matrix, ribbon #3, 500°C after 6 hours
- Figure 15. Al - 25.7 wt % Fe, spherulites

- Figure 16. Selected area diffraction from spherulites in Al matrix (Al 25.7 wt % Fe)
- Figure 17. Details of spherulites, composed of fine crystallites
- Figure 18. Al-34.1 wt % Fe, composed of  $\text{Al}_3\text{Fe}$  in Al matrix
- Figure 19. Selected area diffraction of  $\text{Al}_3\text{Fe}$  phase in Al 34.1 wt % Fe ribbon
- Figure 20. Phase separation in first stage of crystallization of  $\text{Pd}_{77}\text{Si}_{17}\text{Cu}_6$
- Figure 21. Small crystal in  $\text{Pd}_{77}\text{Si}_{17}\text{Cu}_6$  (390°C for 10 min), glassy matrix
- Figure 22. The front of the crystallized eutectic, (390°C for 25 min)
- Figure 23. After 1 hour of exposure to 390°C, the crystallized eutectic spheroidizes
- Figure 24. Ag-15 wt % Cu, microparticles made by the phrasor machine
- Figure 25. Selected area diffraction of particles of Ag-15 wt % Cu.
- Figure 26. Al-1 wt % Mn microparticles, note vacancy clustering

## ABSTRACT

During the reporting period, advances were made in three main areas of study, dealing with the following:

- a. The Al-Fe system
- b.  $\text{Pd}_{77}\text{Si}_{17}\text{Cu}_6$
- c. The Phrasor powders

All three studies are designed to further our understanding of different phenomena that occur in the rapid solidification of useful metallic systems. We now have a better understanding of the structure and the solidification sequence of rapidly solidified Al-Fe alloys containing up to 34 wt % Fe. In rapidly solidified ribbons of  $\text{Pd}_{77}\text{Si}_{17}\text{Cu}_6$  we were able to detect the first stages of crystallization following heat treatments, and then to observe the advancement of the crystallizing front. We had the first look at two of the Phrasor powders, with a particle size which starts at about 3nm, and detected some phenomena which are inherent to the technique.

The only technical problem encountered during the reporting period was related to foil preparation for the Scanning Transmission Electron Microscope (STEM), involving a few alloys, based mainly on silver. These difficulties are expected to be resolved with the purchase of a new ion miller and then these systems will be reinvestigated. In the next reporting period, we plan to finish the work on the first two areas mentioned above and to initiate a study of the Al-Mn and Al-Ti systems using various rapid solidification techniques.

## I. Metastable Phases in the Aluminum-Iron System

### A. Introduction

The aluminum rich side of the Al-Fe phase diagram has been the subject of this study. This side of the diagram indicates the existence of two stable phases, namely aluminum (with a small amount of iron in solid solution) and  $\text{Al}_3\text{Fe}$ . Rapid solidification of Al-Fe compositions within the range of these two phases produces a number of metastable phases, which have been reported in the past, and whose formation depends on the composition of the alloy and on the solidification rate in the various experiments. The following phases have been reported in the literature: (a)  $\text{Al}_6\text{Fe}$ <sup>(1,2)</sup> (b)  $\text{Al}_9\text{Fe}_2$ <sup>(3)</sup> (c)  $\text{Al}_m\text{Fe}$ <sup>(4)</sup> and (d)  $\text{Al}_x\text{Fe}$ <sup>(5)</sup>. Several review papers summarize the information available on the Al-Fe rapidly solidified alloys<sup>(6,7,8)</sup>. The various phases occur in Al-Fe alloys as a function of the cooling rate and can be put in the following order of increasing cooling rate:  $\text{Al}_3\text{Fe}$ ,  $\text{Al}_x\text{Fe}$ ,  $\text{Al}_6\text{Fe}$ ,  $\text{Al}_9\text{Fe}_2$ ,  $\text{Al}_m\text{Fe}$ .

At this time our present study involves three alloys, namely Al 18<sup>W</sup>/o Fe, Al 25.7<sup>W</sup>/o Fe, and Al 34.1<sup>W</sup>/o Fe. The composition of the alloys was designed to probe the rich, hypereutectic Al-Fe diagram, to establish the occurrence of the various phases and to study their thermal stability and transformation. The conditions of the rapid solidification technique prohibit the formation of  $\text{Al}_3\text{Fe}$ ,  $\text{Al}_x\text{Fe}$ , and  $\text{Al}_6\text{Fe}$ .

The expected phases are  $\text{Al}_9\text{Fe}_2$ ,  $\text{Al}_m\text{Fe}$ , or possible unreported phases. However, in compositions richer in iron than  $\text{Al}_6\text{Fe}$ , (like the  $\text{Al}_{34.1}\text{W/oFe}$ )  $\text{Al}_3\text{Fe}$  is likely to form.

B.  $\text{Al}_{18}\text{W/o Fe}$

1. Experimental

The alloy was melt spun using the spinning wheel at the National Bureau of Standards (NBS). Three different ribbons were made using differing wheel speeds and in crucible pressures, as follows.

Ribbon #	Wheel Speed, k rpm	Pressure (psi)
1	14	8.0
2	14	4.0
3	7.6	8.5

Table 1. Spinning conditions for  $\text{Al}_{18}\text{ wt. \% Fe}$

The ribbons obtained were 2mm wide and 0.035 to 0.050mm thick. The slowest cooled ribbon (#3) was given various heat treatments in evacuated vycor tubes, as follows:

Temp., °C	100	300	400	500
Time, hr.	1, 10	1, 10	1, 8	1, 6

Table 2. Heat treatments of ribbon #3

Thin foils for transmission electron microscopy were prepared using a jet electropolishing unit, and standard electrolyte, at  $-40^{\circ}\text{C}$ . All the ribbons were studied in the STEM and the information obtained included general image of the phase structure, selected area and microdiffraction, as well as x-ray analysis of the main phases. Ribbon number 2 was not studied because it had a structure similar to that of ribbon 1.

## 2. Results

### a. Ribbon Number 1

This ribbon, in its as spun condition, has a complex structure of aluminum matrix and at least one other phase, globular in shape. The globular phase, seen in Figure 1 is  $50\mu\text{m}$  in diameter, on the average, and seems to contain large quantities of microcrystallites, as indicated by the rings in the diffraction pattern, Figure 2. These characteristic rings appear in rapidly quenched Al-Fe alloys that contain up to  $25.7^{\text{W}}/\text{oFe}$  ( $14.3^{\text{A}}/\text{oFe}$ ) and probably more (but less than  $34.1^{\text{W}}/\text{oFe}$ , according to our other experiments, as will be shown later). The analysis of the rings will be detailed later when the Al $25.7^{\text{W}}/\text{oFe}$  alloy is reported and in the following discussion. There is no indication in the diffraction pattern that another phase exists in the structure besides the aluminum matrix and the microcrystalline phase.

### b. Ribbon Number 3

In its as spun condition, Ribbon Number 3 contains three phases, namely Al $\frac{1}{3}$ Fe, the globular phase, and cellular

aluminum matrix. The fine crystallites that form in the globular phase appear to have the same crystallography as the cell boundaries of the matrix. Figure 3 shows an  $\text{Al}_3\text{Fe}$  particle. Its cross-section has a characteristic flower shape, and the concentration of these particles in the ribbon is very low. The globular phase, the quantity of which is much larger, is shown in Figure 4. This phase has an average diameter of  $0.25\mu\text{m}$ . The matrix shown in Figure 4 is aluminum and the cell size is less than  $100\text{nm}$ . The chemical composition of this phase and the matrix is given in Figures 8 and 9, respectively. The crystallographic characteristics of the globular phase was found to be different for various particles. Two microdiffraction patterns of these particles are shown in Figure 5 and 6. The first is entirely crystalline with no indication of ring pattern. The second, taken from a particle that looks very similar, is characteristic of very fine crystalline structure. Figure 6 was taken of a particle marked in Figure 7. A close observation shows some diffraction contrast in the particle, which may suggest that under the solidification conditions of this ribbon the globules are partially amorphous and contain fine crystallites.

The composition analysis of the globular phase was done by the EDAX system on the STEM. The results shown in Figure 8 indicate that the composition of the phase is close to  $\text{Al}_6\text{Fe}$ . The composition of the background is given in Figure 9 and is the average of the composition of the aluminum matrix and that of the cells in it.

The nature of the formation of the globular phase may be the key to the understanding of the solidification process in aluminum alloys rich in iron. Our understanding of this phase and the mechanism of its formation as well as the surrounding matrix is not complete at this time. At this stage, it appears that the molten alloy separates into two phases, one of which is richer in iron ( $25.57^w/o$ ), and the other one, leaner in iron ( $14.1^w/o$ ). The richer phase may be the first to solidify, forming globules, and the leaner phase, solidifying later, has the characteristic cellular structure, that forms the matrix.

Specimens of ribbon number 3 that were annealed for 10 hours at  $300^\circ C$  did not show any significant difference from the as spun ribbon. The phase structure was found to be the same, and the average size of the globules was still  $0.25\mu m$ . The selected area diffraction pattern contains rings which originate at the cell boundaries of the aluminum matrix. The heat treatment was found to effect the ordering of the globular phase, which at this stage is completely ordered, as can be seen in the example of the lattice image, Figure 10. At  $400^\circ C$ , in the first hour of exposure, needles of  $Al_3Fe$  start to appear, while the globules dissolve. This occurs first in regions close to the previously existing  $Al_3Fe$  (Figure 11). After 8 hours at  $400^\circ C$  the specimen is composed of  $Al_3Fe$  needles in  $Al$  matrix, Figure 12. Very few traces of globules can be detected at this stage. The  $Al_3Fe$  particles contain planar faults which run either parallel or perpendicular to their long axis. At  $500^\circ C$ ,

following 1 hour of exposure the foil contains mainly  $\text{Al}_3\text{Fe}$  needles, but traces of globules can be resolved (Figure 13). After 6 hours at this temperature only  $\text{Al}_3\text{Fe}$  particles can be found, as shown in Figure 14.

C.  $\text{Al}_{25.7}^{\text{W}}/\text{oFe}$

A ribbon, the composition of which corresponds to the metastable precipitate  $\text{Al}_6\text{Fe}$ , was spun with a wheel speed of 6000 rpm and a tube pressure of 8 psi. The ribbon thus obtained measured 50  $\mu\text{m}$  in thickness and 2mm in width.

The microstructure as observed in the STEM contains mainly spherulites, the average size of which is 0.7  $\mu\text{m}$  in diameter. Some aluminum matrix can be found between these spherulites. Figure 15 presents a general view of the microstructure and Figure 16, the corresponding diffraction pattern. A detailed image of one of the particles is shown in Figure 17. Each spherulite is a polycrystalline aggregate of microcrystallites as can be observed both in Figure 17 and in the selected area diffraction pattern, Figure 16. The following Table 3 summarizes the ring diameters and the corresponding d spacing of the spherulitic phase in this alloy.

Ring #	1	2	3	4	5	6	7	8	9	10	11
2R [cm]	1.3	1.47	2.0	2.2	2.5	2.8	3.55	4.05	4.25	4.75	4.95
d, Å	3.96	3.50	2.58	2.34	2.06	1.84	1.45	1.27	1.21	1.08	1.04

Table 3. The ring diameters shown in Figure 16 and the corresponding d spacings

The x-ray diffraction pattern obtained from the ribbon provided confirmation for most of the rings and additional detail of some of them. The strong ring, #5, is subdivided into 3 (or 4) rings which represent the following d spacings: 2.03, 2.06, and 2.09 Å.

The identity of this phase, which appear in both the 18 w/o Fe and in the 25.7 w/o Fe is unclear at this time. It is, however, apparent that it is none of the following:  $\text{Al}_3\text{Fe}$ ,  $\text{Al}_6\text{Fe}$ ,  $\text{Al}_9\text{Fe}_2$ , or  $\text{Al}_x\text{Fe}$ , or  $\text{Al}_m\text{Fe}$ .

D.  $\text{Al}_{34.1}\text{W/oFe}$  ( $\text{Al}_{80}\text{Fe}_{20}$ )

In an attempt to establish the upper limit of Fe concentration that will still form the globular phase on rapid solidification, this composition was melt spun, at 6000 rpm and 9 psi. The ribbon thus formed is flaky in appearance and is very brittle. X-ray diffractometry established its composition to be  $\text{Al}_3\text{Fe}$  and a small amount of Al. TEM foils revealed its structure to be lamellar, probably as eutectic of elongated  $\text{Al}_3\text{Fe}$  crystals. These contain planar faults, generally perpendicular to their growth direction, as can be seen in Figure 19. A diffraction pattern of this structure is shown in Figure 19. No trace of the globular phase could be detected in this alloy.

### E. Discussion

Of all the aluminum binary systems, rapidly solidified Al-Fe alloys were the ones most reported in the literature. However, the compositions studied were low in iron content. Examples are: up to 4.4 at % <sup>(9)</sup>, 2 at % <sup>(10)</sup>, up to 6 at % <sup>(11)</sup>, 8 wt % ( $\sim$ 4 at %) <sup>(12)</sup>, up to 6.1 wt %, ( $\sim$ 3 at %) <sup>(13)</sup>, and 0.5 wt % (0.24 at %) <sup>(14)</sup>. H. Jones <sup>(15)</sup> investigated a wide variety of Al-Fe compositions, up to 32.9 wt % Fe (19.15 at %), but he studied only composition up to 11 wt % (5.6 at % Fe) in the TEM. Jacobs and coauthors <sup>(12)</sup> analyzed the electron diffraction rings generated from an Al 8 wt % alloy as representing a cubic phase with a cell parameter of 0.360nm. Our study is able to confirm most of the reported rings, however, a detailed examination of our patterns, identical for the two compositions studied, shows more rings, some of which were not reported by Jacobs <sup>(12)</sup>. Our x-ray diffraction analysis further confirmed the TEM diffraction patterns, and the results suggest that the structure of the globules and the cell boundaries in the aluminum matrix is more complex.

The disappearance of the globular phase and the formation of Al<sub>3</sub>Fe needles suggests that there is no intermediate phase, and upon dissolving, the Al-18 wt % Fe does not form Al<sub>6</sub>Fe. Only three phases could be detected in all the alloys investigated, namely, Al, Al<sub>3</sub>Fe and an unidentified phase, very fine in shape, which occurs in the cell boundaries and

in the globular particles found in the alloys Al-18 wt % Fe, and Al 25.7 wt % Fe.

## II. The Crystallization of $\text{Pd}_{77}\text{Si}_{17}\text{Cu}_6$

Glassy ribbons of  $\text{Pd}_{77}\text{Si}_{17}\text{Cu}_6$  were made by melt spinning at the NBS facility under conditions similar to the preparation of the other ribbons. The ribbons were annealed at 390°C for various periods of time. A selected group of the specimens were studied by transmission electron microscopy. The group included specimens that were soaked, at the specified temperature for 5, 10, 25 and 60 min. (specimen number 0, 1, 5, 9) respectively). Treatment for 5 min. resulted in a phase separation (Figure 20), in isolated areas. The size of the separated phases was too small to make it possible to analyze the samples with the EDAX system of the STEM. The region, about 100nm in diameter, is separated into two glassy phases, one light and the other dark. Crystallites, a few nm in size, appear in the darker phase. Since phase separation has not been reported in this material, and because of the minute size of the area, no definitive conclusion could be drawn about the exact nature of the phenomenon, even though the same phenomenon has been observed in a few areas. More work will have to be done before a satisfactory explanation can be given. A 10 min. treatment at 390°C generated a typical eutectic structure. Under these conditions, the crystals start to grow in various sites such as shown in Figure 21. The eutectic has been analyzed and reported earlier by Boettinger<sup>(16,17)</sup>.

The eutectic colonies are about  $1\mu\text{m}$  in diameter at this stage and form a crystalline mass about  $3\mu\text{m}$  in diameter. Further growth of the crystalline eutectic phase is observed in a specimen that was exposed to the referenced temperature for 25 min. The front of the crystallized eutectic is shown in Figure 22. After one hour of exposure at  $390^{\circ}\text{C}$ , the eutectic starts to form spheroids as is demonstrated in Figure 23.

### III. Rapidly solidified powders generated by the Micro Particle Processor (Phrasor)

Two powders have been produced and studied utilizing the micro particle processor (Phrasor, Duarte, California). The composition of the powders are Ag-15 wt % Cu and Al-1 wt % Mn. An example of the first powder is shown in Figure 24, and a diffraction pattern is presented in Figure 25. The process generates particles whose size starts at 3nm. The particles are single crystals, and only rarely double crystals. They show diffraction contrast but no faults or any other structural details. The particles are well separated from one another due to the static electric charge which they contain. Larger particles while also charged fall onto the substrate and by virtue of their increased mass can come to rest on top of some of the smaller particles despite their electric charge. Smaller particles that are produced after this point will be repelled by the electric field generated by the larger particles and will fall in an isolated pattern away from the neighboring particles (Figure 24). The second alloy, Al-1 wt % Mn, contains

particles with the same geometrical characteristics. A detailed look at these larger particles reveals a high density of vacancy clustering at the interior of the particles (Figure 26). No cell formation could be observed in any of the particles. This is to be expected due to the high solubility reported for Mn in rapidly quenched aluminum-9 wt %<sup>(18)</sup>. A further study is planned with other Al-Mn alloys.

Acknowledgement

The authors wish to acknowledge the contributions of F. Biancaniello for specimen preparation and J. Cahn, R. Mehrabian, W. J. Boettinger and M. Rosen for helpful discussions. We also gratefully acknowledge the valuable technical discussion and assistance of Lt. Col. J. Jacobson of DARPA.

REFERENCES

1. E. H. Hollingsworth, G. R. Frank and R. E. Willett, Trans TMS-AIME 234 (1962) 188.
2. L. K. Walford, Acta Cryst. 18 (1965) 287.
3. C. J. Simensen and R. Vellamy, Z Metallk, 68 (1977) 428.
4. I. Miki, H. Kosuge and N. Nagahama, J. Jap. Inst. Light Metals, 25 (1975) 1.
5. R.M.K. Young and T. W. Clyne, Scripta Met. 15 (1981) 1211.
6. H. Jones, Mater. Sci. Eng. 5 (1969) 1.
7. I. R. Hughes and H. Jones, J Mat. Sci. 11 (1976) 1711.
8. T. R. Anantharaman et al. Trans Indian Inst of Metals 30 (1977) 423.
9. A. Tonejo and A. Bonefacic, J Appl. Phys 40 (1969) 419.
10. E. Blank, Z. Metallk, 63 (1972) 315.
11. P. Furrer and H. Warlimont, Z Metallk. 64 (1973) 236.
12. M. H. Jacobs, A. G. Doggett and M. J. Stowell, J. Mater. Sci. 9 (1974) 1631.
13. I. R. Hughes and H. Jones, J Mat. Sci. 11 (1976) 1781.
14. C. J. Simensen and R. Vellamy, Z Metallk. 68 (1977) 428.
15. H. Jones, Mater. Sci. Eng. 5 (1969/70) 1.
16. W. J. Boettinger, Forth International Conference on Rapidly Quenched Metals, 1981 Sendai, Japan.
17. Boettinger and Ives on PdCuSi, Private Communication.
18. N. J. Grant, Fizika, 2 (Suppl. 2) (1970) Paper No. 16.

APPENDIX 1

(Figures 1-26)

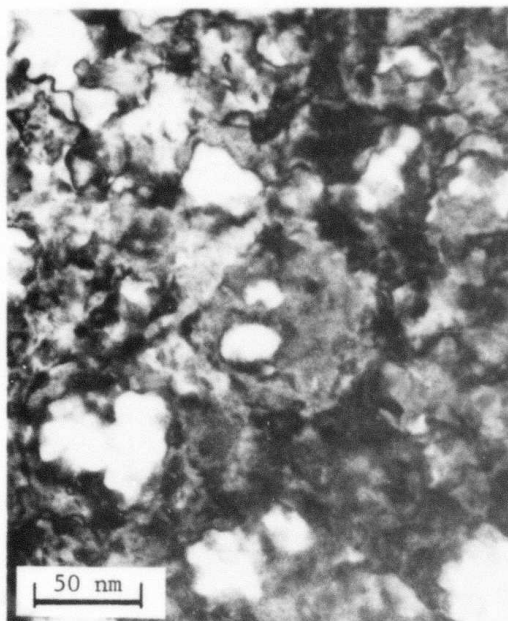


FIGURE 1  
The globular phase in Al 18 wt %  
Fe (ribbon #1)



FIGURE 2  
Selected area diffraction ring pattern  
from ribbon #1

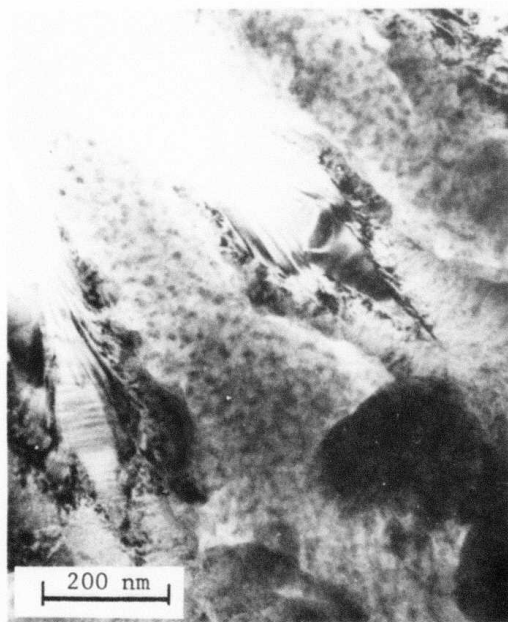


FIGURE 3  
 $\text{Al}_3\text{Fe}$  particle in ribbon #3

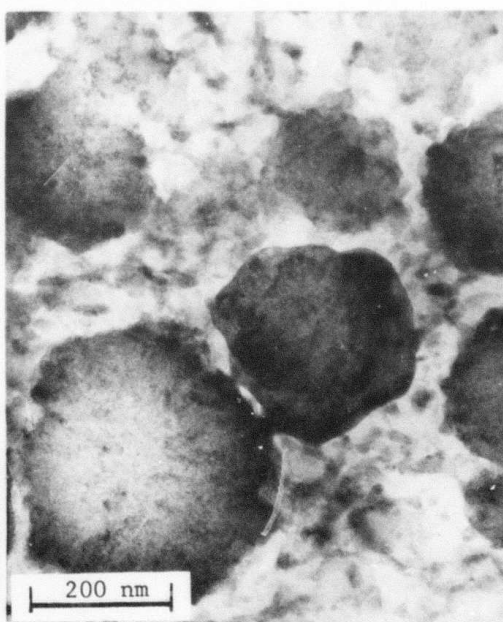


FIGURE 4  
The globular phase in ribbon #3



FIGURE 5  
Microdiffraction from globular  
phase - crystalline



FIGURE 6  
Microdiffraction from globular  
phase - microcrystalline

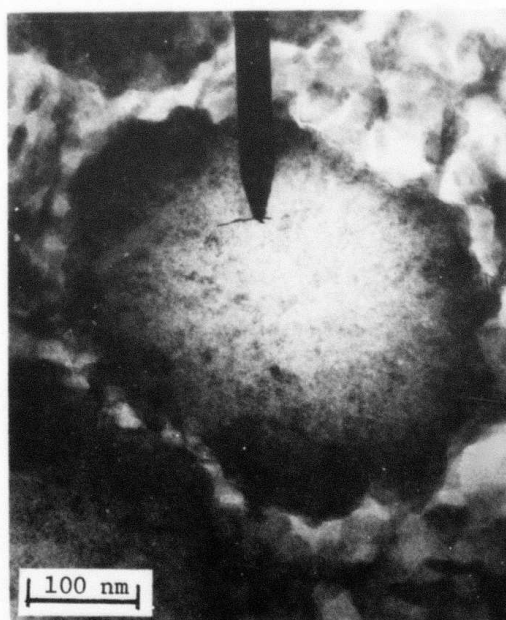


FIGURE 7  
Microcrystallites formed in globular  
phase

AL18FE  
 KV=25. tilt=30. tkoff=15.  
 BKG Pt1= 2.0 BKG Pt2=17.3  
 NOST  
 22-SEP-81

# CONCENTRATION

	WT. %	AT. %	% S. E.
ALK	74.33	85.70	1.13
FEK	25.67	14.30	2.12
-----			
	100.00		

22-SEP-81 12:14:14 QUANTITATIVE  
 RATE: 66082CPS TIME: 200LSEC  
 00-20KEV:10EV/CH PRST: OFF  
 A:AL18FE B:  
 FS= 902 MEM: A FS= 1000

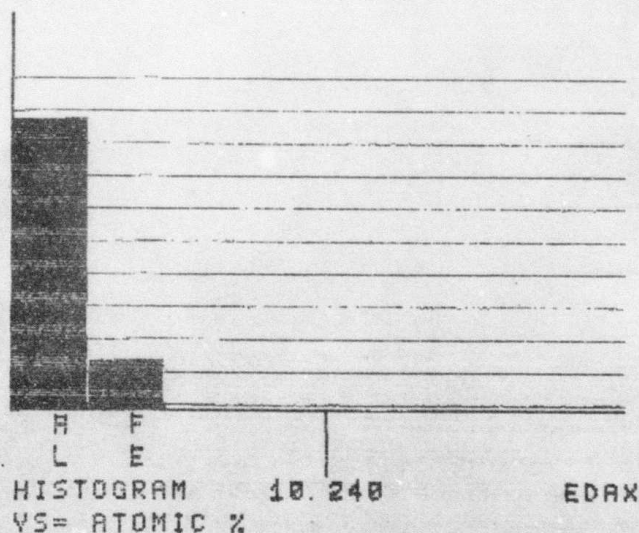


FIGURE 8

Composition of the globular phase (EDAX on STEM)

AL IN AL18F4  
 KV=25. TILT=30. TKOFF=15.  
 BKG P1= 2.0 BKG P2=17.3  
 NOST  
 22-SEP-81

# CONCENTRATION

	WT. %	AT. %	% S. E.
ALK	95.90	92.65	1.16
FEK	4.10	7.35	3.70
-----			
	100.00		

22-SEP-81 04:29:03 EDAX READY  
 RATE: 107CPS TIME: 200LSEC  
 00-20KEV:10EV/CH PRST: OFF  
 A:AL IN AL18F4 B:  
 FS= 1032 MEM: A FS= 200  
 00 02 04 06 08

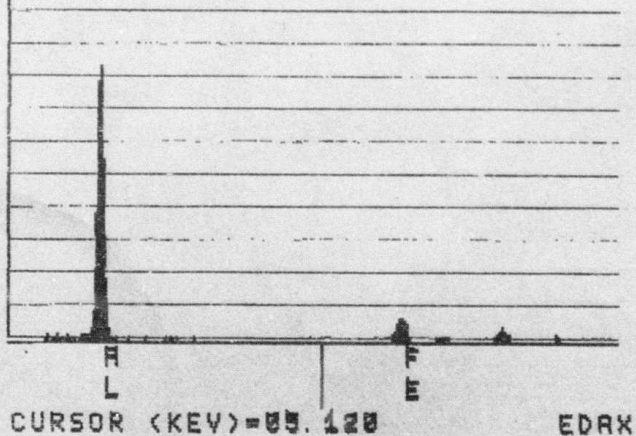


FIGURE 9

Composition of matrix (cells and cell boundaries) (EDAX on STEM)

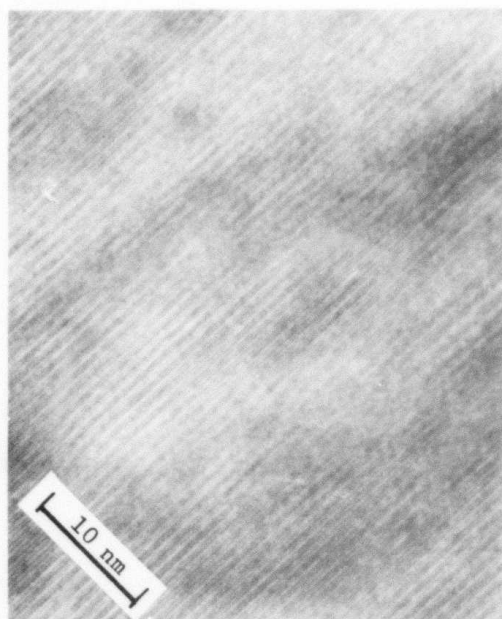


FIGURE 10

Lattice imaging of ordered globules in ribbon #3 (300°C-10h)



FIGURE 11

First  $\text{Al}_3\text{Fe}$  needles to appear in ribbon #3 (400°C-1h)



FIGURE 12

$\text{Al}_3\text{Fe}$  in Al matrix is characteristic of ribbon #3 after 8 hours at 400°C



FIGURE 13

Ribbon #3, 1 hour at 500°C, Al matrix and  $\text{Al}_3\text{Fe}$  but some globules still exist



FIGURE 14

$\text{Al}_3\text{Fe}$  in Al matrix, ribbon #3, 500°C  
after 6 hours

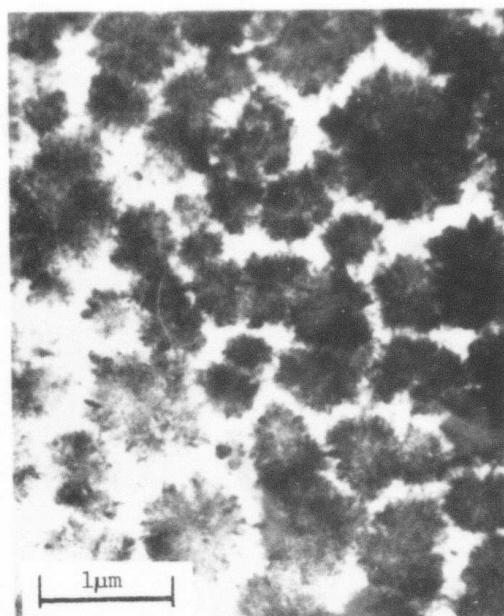


FIGURE 15

Al - 25.7 wt % Fe, spherulites



FIGURE 16

Selected area diffraction from  
spherulites in Al matrix (Al 25.7  
wt % Fe)

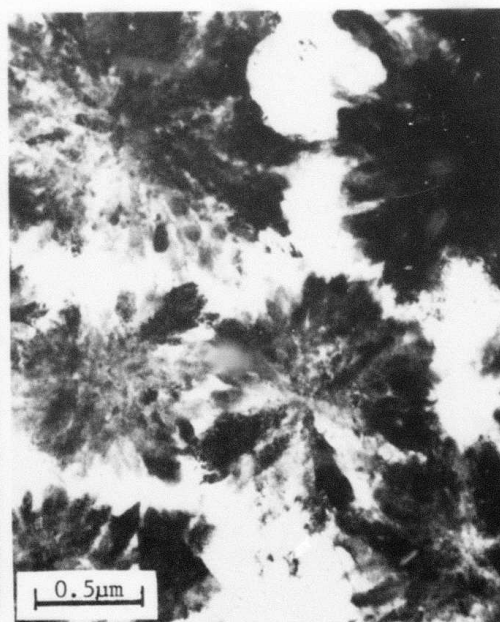


FIGURE 17

Details of spherulites, composed of  
fine crystallites

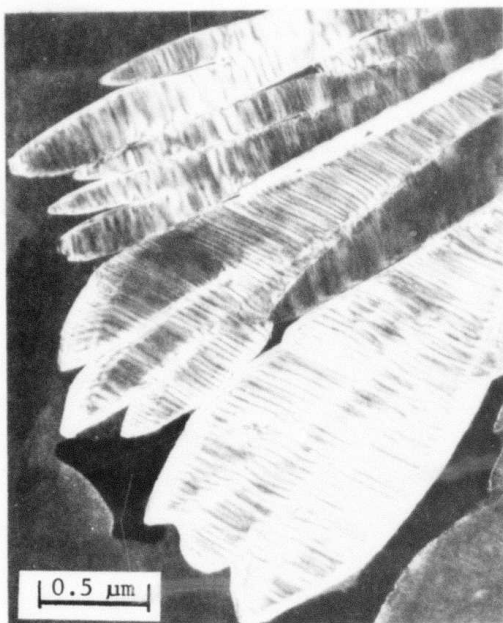


FIGURE 18  
Al-34.1 wt % Fe, composed of  $\text{Al}_3\text{Fe}$   
in Al matrix

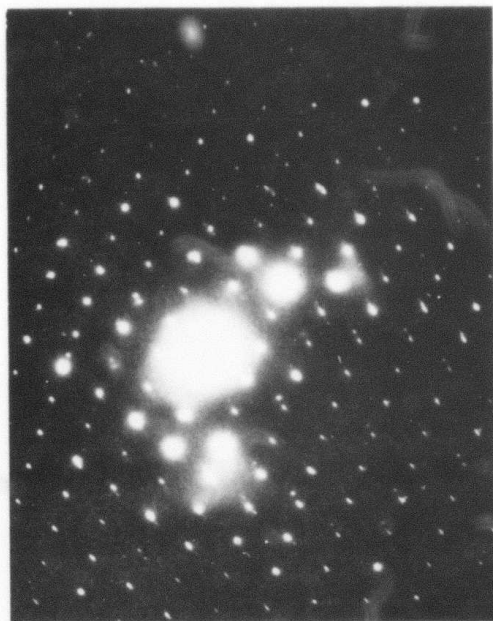


FIGURE 19  
Selected area diffraction of  $\text{Al}_3\text{Fe}$   
phase in Al 34.1 wt % Fe ribbon

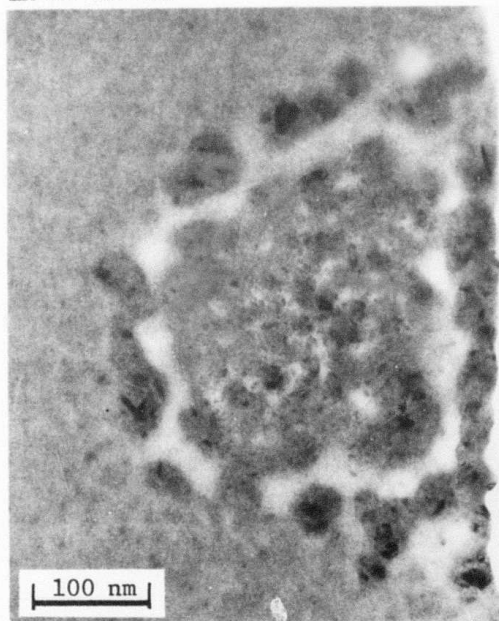


FIGURE 20  
Phase separation in first stage of  
crystallization of  $\text{Pd}_{77}\text{Si}_{17}\text{Cu}_6$



FIGURE 21  
Small crystal in  $\text{Pd}_{77}\text{Si}_{17}\text{Cu}_6$  (390°C for  
10 min), glassy matrix



FIGURE 22

The front of the crystallized eutectic (390°C for 25 min)

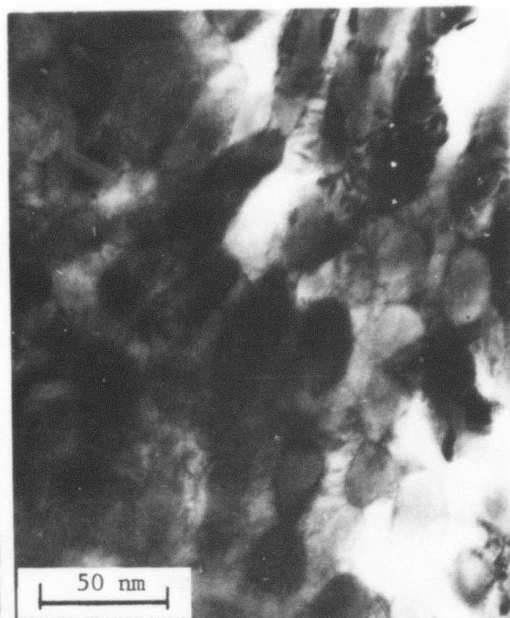


FIGURE 23

After 1 hour of exposure to 390°C, the crystallized eutectic spheroidizes

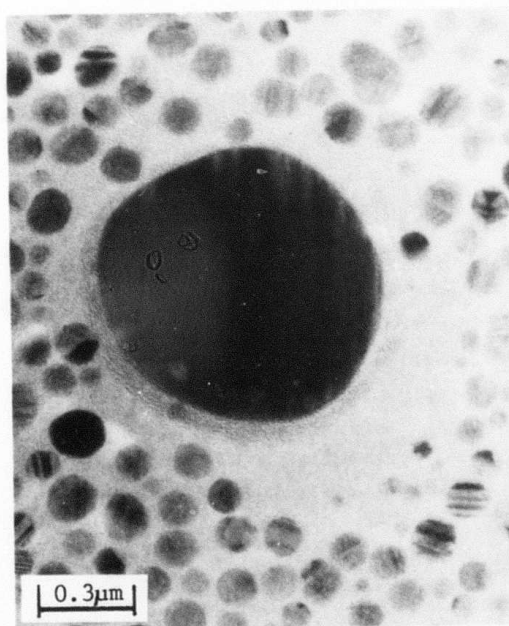


FIGURE 24

Ag-15 wt % Cu, microparticles made by the phrasor machine

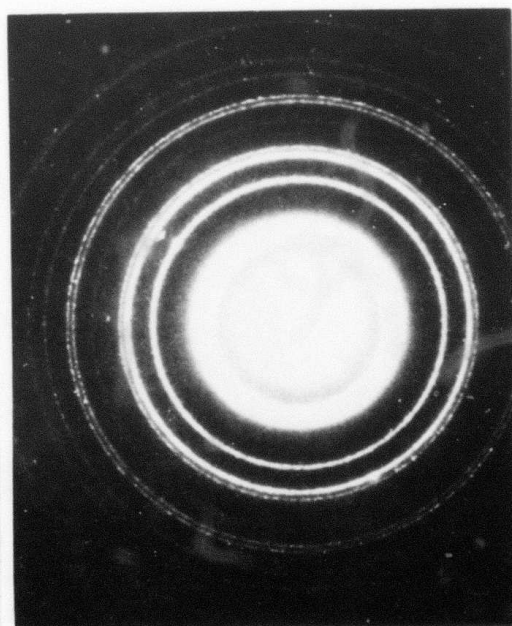


FIGURE 25

Selected area diffraction of particles of Ag-15 wt % Cu

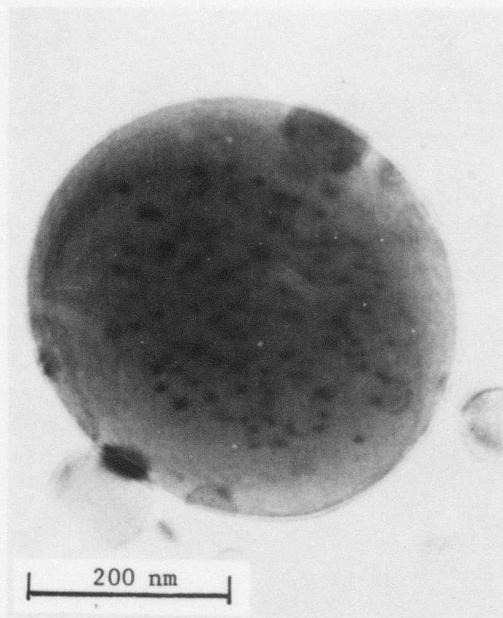


FIGURE 26

Al-1 wt % Mn microparticles, note  
vacancy clustering